Equireflectionality and customized unbalanced coherent perfect absorption in asymmetric waveguide networks

Malte Röntgen, Olivier Richoux, Georgios Theocharis, Christian V Morfonios, Peter Schmelcher, Philipp del Hougne, Vassos Achilleos

Equireflectionality and customized unbalanced coherent perfect absorption in asymmetric waveguide networks

Malte Röntgen,[1,2] Olivier Richoux,[2] Georgios Theocharis,[2] Christian V. Morfonios,[1] Peter Schmelcher,[1,3] Philipp del Hougne,[4] and Vassos Achilleos[2]

[1] *Zentrum für optische Quantentechnologien, Universität Hamburg, Luruper Chaussee 149, 22761 Hamburg, Germany*
[2] *Laboratoire d'Acoustique de l'Université du Mans, Unite Mixte de Recherche 6613, Centre National de la Recherche Scientifique, Avenue O. Messiaen, F-72085 Le Mans Cedex 9, France*
[3] *The Hamburg Centre for Ultrafast Imaging, Universität Hamburg, Luruper Chaussee 149, 22761 Hamburg, Germany*
[4] *Univ Rennes, CNRS, IETR-UMR 6164, F-35000 Rennes, France*

We explore the scattering of waves in designed asymmetric one-dimensional waveguide networks. We show that the reflection between two ports of an asymmetric network can be identical over a broad frequency range, as if the network was mirror-symmetric, under the condition of so-called *latent* symmetry between the ports. This broadband equireflectionality is validated numerically for acoustic waveguides and experimentally through measurements on microwave transmission-line networks. In addition, introducing a generalization of latent symmetry, we study the properties of an N-port scattering matrix S. When the powers of S fulfill certain relations, which we coin *scaled cospectrality*, the setup is guaranteed to possess at least one zero eigenvalue of S, so that the setup features coherent perfect absorption. More importantly, scaled cospectrality introduces a scaling factor which controls the asymmetry of the incoming wave to be absorbed. Our findings introduce a novel approach for designing tunable wave manipulation devices in asymmetric setups. As evidenced by our acoustic simulations and microwave experiments, the generality of our approach extends its potential applications to a wide range of physical systems.

I. INTRODUCTION

Scattering of waves is unambiguously of fundamental importance in physics, finding applications in fields as diverse as high-energy physics [1], X-ray diffraction [2], wave localization [3] or wave filtering [4–6]. In any scattering problem, the system's symmetries have a strong influence. For a reflection symmetry—the simplest geometric symmetry—, for instance, waves sent into the system from the two opposite sides of the symmetry axis (or plane) act identically, thus the two reflection coefficents are strictly equal.

Here, on the other hand, we are interested in exploring the scattering properties of geometrically *asymmetric* systems. In particular, we focus on systems featuring the recently introduced *latent symmetry* [7–9]. Such a symmetry is usually not visible in the original setup, but it becomes apparent after a suitable dimensional reduction, the so-called isospectral reduction [10]. What is interesting about a latent symmetry is its strong impact on the eigenmodes of the underlying system [11]. A latent reflection symmetry, for instance, induces local parity on the eigenvectors of the underlying matrix M describing the system (for instance, the Hamiltonian or the scattering matrix) [8, 12, 13].

Interestingly, the impact of a latent symmetry goes beyond the system's eigenvectors and manifests itself also in certain relations of the powers of the matrix M [14]. For a latent reflection symmetry with respect to two sites u, v, the corresponding diagonal elements $\left(M^k\right)_{u,u}$ and $\left(M^k\right)_{v,v}$ of the matrix powers of M are the same for all positive integers k [8]. On a fundamental level, this result is interesting, as it shows a deep connection between the powers of M and its eigenvectors [12].

In the first part of this work, we carry the concepts of latent symmetry and of matrix powers to the realm of wave scattering. We start by applying the concept of latent symmetry to design geometrically *asymmetric* systems whose scattering properties carry the same traits as a reflection symmetric system, that is, broadband equireflectionality. We validate this intriguing property numerically in acoustic waveguide networks and experimentally in microwave transmission-line networks.

Then, in the second part of this work, we explore the impact of relations in the matrix powers of a general scattering matrix. Specifically, we show that an N-port system can be designed to feature coherent perfect absorption (CPA) using *scaled* matrix power relations. CPA implies the complete and irreversible transduction of the incident wave energy into other degrees of freedom such as heat, which is possible whenever the scattering matrix has a zero eigenvalue and the corresponding eigenvector is used as incident wavefront [15]. This condition is valid irrespective of the complexity of the wave system, applying to simple [16] or disordered [17] systems excited by a single channel as well as simple [18] or disordered [19] systems excited by multiple channels. In asymmetric disordered systems, the necessary wavefront is generally very complex unless the system is optimized to impose CPA with a specific wavefront [20]. Here, we show that a 3-port system designed to feature scaled cospectral-

ity will enable CPA with a prescribed imbalance of the corresponding wavefront that is controlled by tuning the associated scaling factor.

This paper is organized is follows. Section II is dedicated to the concept of equireflectional scattering, including theoretical and experimental verifications of the theory. Section III focuses on the powers of the scattering matrix of a generic N-port setup. In particular, we introduce scaled matrix power relations which can be directly related to CPA. We then focus on a simple three-port system, which we optimize to feature scaled cospectrality and hence CPA with custom imbalance of the CPA wavefront. Finally, we conclude our work in Section IV.

II. SCATTERING OFF LATENTLY SYMMETRIC NETWORKS

In the following, we will discuss how a latent reflection symmetry leads to equireflectional scattering. After introducing this phenomenon by means of a simple example in Section II A, we show in Section II B how this phenomenon can be explained and designed; in Section II C and Section II D we numerically and experimentally validate our findings with acoustic waveguide and microwave transmission-line networks, respectively.

A. Setup and a first example

Consider a general reciprocal two port system, with only a single mode traveling within each lead/port as depicted in Fig. 1(a). This problem is characterized by the following scattering matrix equation

$$\begin{pmatrix}\psi_1^-\\ \psi_2^-\end{pmatrix} = \begin{pmatrix} r_1 & t\\ t & r_2\end{pmatrix}\begin{pmatrix}\psi_1^+\\ \psi_2^+\end{pmatrix} = S\begin{pmatrix}\psi_1^+\\ \psi_2^+\end{pmatrix}, \qquad (1)$$

where $(\psi_1^-,\psi_2^-)^T$ and $(\psi_1^+,\psi_2^+)^T$ describe, respectively, the output and input waves. The off-diagonal elements of S correspond to the transmission coefficients from left and right which, here, are equal due to reciprocity ($S = S^T$ is symmetric with respect to the diagonal). The reflection coefficients from ports 1 and 2 are noted respectively r_1 and r_2.

In this section, we consider networks of identical one-dimensional waveguide segments with the same length L, such as the ones shown in Fig. 1(b-d). We note that networks of one-dimensional waveguides are known as "quantum graphs" and have been studied extensively in the last decades; an excellent introduction to the field is given in [22]. Experimentally, they could be realized, for instance, in the form of microwave networks [23, 24] or networks of thin acoustic waveguides [13, 25, 26]; in this paper, we will focus on the former for our experimental validation, while we focus on the latter for our numerical results.

Let us now investigate the scattering off such a waveguide network, and focus on the behavior of the reflection

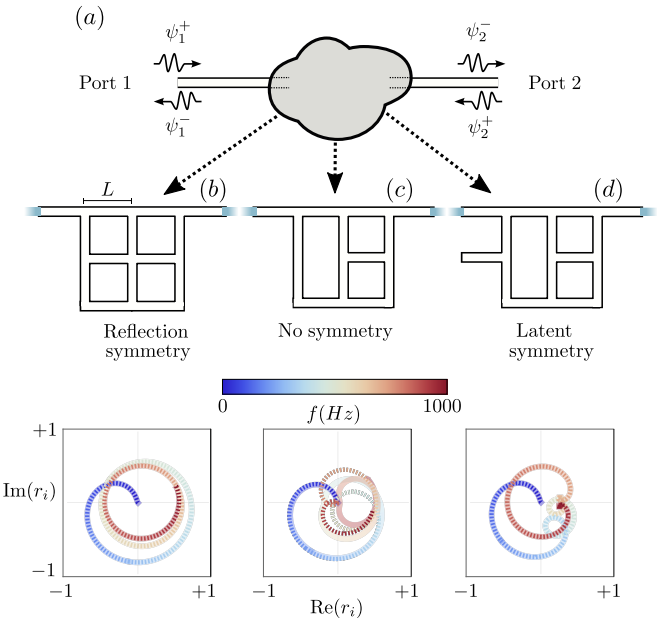

Figure 1. (a) A generic two-port scattering setup. (b-d): Different waveguide networks (upper panel) with their respective frequency-dependent reflection coefficients $r_1(f)$ (solid line), $r_2(f)$ (dashed line) in the complex plane shown in the lower subpanel. These reflection coefficients have been computed using the method from [21] for acoustic waves with visco-thermal losses (Eqs. (E1) and (E2) with loss-coefficient $\alpha = 3{\cdot}10^{-5}$), with a frequency f between 0 and 1000 Hz. Each waveguide has a length $L = 0.1m$ and a diameter $R = 2mm$.

coefficients r_1 (from left) and r_2 (from right). To do so, here, we consider 1D acoustic waves of frequency $\omega = c_0 k$ where c_0 is the sound speed and k the wavenumber. The reflection of the two-port system is given by the scattering matrix calculated using the 1D Helmholtz equation in each waveguide and the conservation of acoustic flux at the connections [21, 27]; an explicit expression for the scattering matrix is given in Appendix A. Note that this $1D$ approximation is valid for acoustic propagation through the waveguides, assuming that $L \gg w$, where L (w) is the length (width) of each waveguide.

For a mirror-symmetric network, we expect *equireflectionality*, that is, $r_1 = r_2$, simply due to the total symmetry of the scattering problem. For illustration purposes, we show the two reflection coefficients of the network of Fig. 1(b) in the complex plane in the bottom panel, verifying equireflectionality. Notice that here we have considered the effect of homogeneously distributed losses since the reflection coefficients are inside the unit circle (see below for details). Evidently, such losses maintain the mirror symmetry.

Breaking this mirror symmetry, as is the case in Fig. 1(c), is expected to destroy equireflectionality. That is, $r_1 \neq r_2$ except for some special frequencies where the two reflection coefficients coincide. This is clearly seen in the bottom panel in Fig. 1(c). On the other hand, for a special *asymmetric* setup as the one in Fig. 1(d) we

find that the system *is* equireflectional, *i.e.*, $r_1 = r_2$, as shown in the bottom panel, even in the presence of losses. This surprising result is not obtained by chance or coincidence. In fact, below, we show how such asymmetric equireflectional networks can be designed, and how their equireflectionality can be explained through the recently introduced concept of latent symmetry.

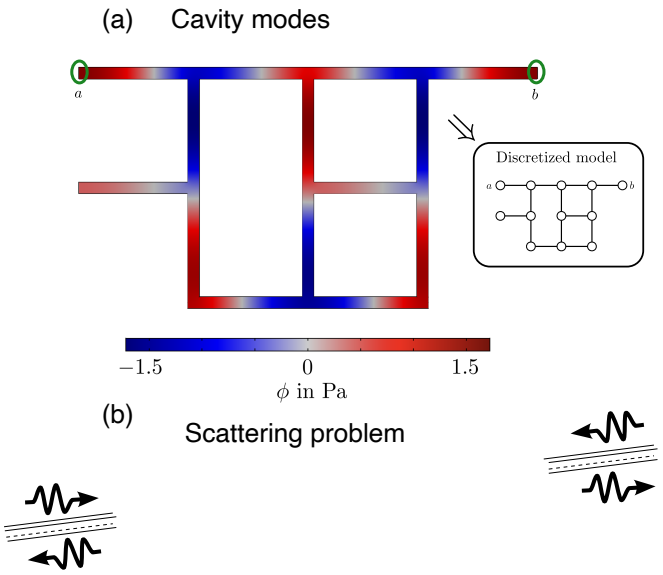

Figure 2. The network of Fig. 1 (d), realized with thin, square-shaped acoustic waveguides of length $L = 0.1m$ and side length $w = 10mm$ (see Section II C for details). (a) The 10th mode of the acoustic network with closed ends. The inset shows the corresponding discrete model (graph). (b) Schematic of the scattering process by the 2-port network. The acoustic pressure field here corresponds to a symmetric input (same amplitude and phase) from both ports at $f = 625$Hz.

B. Review of latent symmetry in waveguide networks

To understand the highly symmetric scattering properties of the setup depicted in Fig. 1(d), we first need to study the eigenmodes of the corresponding cavity that is obtained by closing the connections to the leads, as shown in Fig. 2.

Before we start our theoretical treatment, let us briefly inspect Fig. 2 (a) in more detail. There, we show the wavefield of one of the cavity's eigenmodes. As can be seen, this mode is, to a good approximation, a plane-wave mode: While the wave field changes along a given waveguide (longitudinal direction), it is constant along its transverse direction. This is, of course, expected from the fact that our narrow waveguides are effectively one-dimensional only.

What is interesting about the eigenmode ϕ depicted in Fig. 2 (a) is that its amplitudes at the two points a and b are the same. This is no coincidence. Indeed, as we shall show below, *all* eigenmodes of the cavity fulfill either $\phi(a) = \phi(b)$ or $\phi(a) = -\phi(b)$. In other words, the eigenmodes show *point-wise* parity at the two points a, b. We note that this property for acoustic waveguides has been studied in detail in Ref. [13] and here we review the basic results.

The basic idea for finding the eigenmodes of the waveguide network is then as follows: Since our waveguides are effectively one-dimensional, knowledge of the wave field only at at the junctions and at end point (like a, b) of the network is sufficient to reconstruct the wavefield in the entire network. Thus, we can simplify the problem by discretizing the network, as shown in the inset of Fig. 2 (a). The discrete model is nothing but a graph: A collection of points (vertices)—each of them corresponding to a junction or to a waveguide endpoint—interconnected by lines (edges), each of which representing a waveguide.

Following the above idea of discretizing the problem, as sketched above, it can be shown that the problem of finding the eigenmodes ϕ of the network is equivalent to the following generalized eigenvalue problem

$$A\,\boldsymbol{\phi} = \cos(kL) B\,\boldsymbol{\phi} \tag{2}$$

with $\cos(kL)$ being the eigenvalue, the N-dimensional eigenvector $\boldsymbol{\phi}$ denoting the values of the eigenmode ϕ at the N vertices. The matrix A describes the topology of the setup, with $A_{i,j} = 1$ if the vertices i, j are connected by a waveguide, and $A_{i,j} = 0$ otherwise. The matrix B is diagonal, with $B_{i,i} = \sum_j A_{i,j}$. We then introduce the "Hamiltonian" $H = \sqrt{B}^{-1} A \sqrt{B}^{-1}$, which arises naturally from Eq. (2) through the transformation $\mathbf{y} = \sqrt{B}\boldsymbol{\phi}$.

We are then left with the eigenvalue problem

$$H\mathbf{y} = \cos(kL)\mathbf{y}\,. \tag{3}$$

Solving Eq. (3) gives us the natural frequencies of the eigenmodes for the network cavity, as well as the values of the field at the nodes.

The claim is that, there are two different ways [13] to obtain point-wise parity at some points a, b for all eigenmodes. The first is through geometrical symmetry, that is, when the system is invariant under a symmetry operation—usually a reflection, as is the case for Fig. 1 (a)—which maps the junctions a and b onto each other. The second and non-obvious case occurs when the setup is *not* invariant under a geometrical operation that maps a and b onto each other. This is the case for the network of Fig. 2 (a) and Fig. 1 (d). In fact, the corresponding discrete network, as shown in the inset of Fig. 2 (a),

has been designed such that the following relation of the matrix powers of H is fulfilled

$$(H^m)_{a,a} = (H^m)_{b,b} \tag{4}$$

for $m = 1, \ldots, N$. This has been found to ensure the pointwise parity of a and b for all the modes [13]. Note that Eq. (4) is automatically satisfied for a mirror symmetric setup. As we demonstrate in Appendix D, the relations Eq. (4) can also be translated into a set of geometric rules that can be visually checked. The simplest of these rules says that the number of neighbors of points a and b—that is, the number of waveguide that are directly connected to these points—have to be the same. For the network of Fig. 2 (a), both a and b have only one neighbor.

Interestingly, the relations Eq. (4) have also a consequence on eigenvalues: If a matrix H satifies these, then the two matrices $H \setminus a$ and $H \setminus b$—obtained from H by removing the ath (or bth) row and column—have the same eigenvalue spectra. We thus say that a and b are *cospectral*.

Before continuing, let us mention that the relations Eq. (4) lead to another very interesting consequence. By performing a certain dimensional reduction onto the two sites $\{a, b\}$—the so-called isospectral reduction [10], the resulting reduced system can be described by an effective Hamiltonian with a reflection symmetry. This explains the point-wise parity of eigenvectors on a, b. Since this symmetry becomes in general only apparent after the dimensional reduction, we call the Hamiltonian H *latently reflection symmetric* [7, 11, 13].

C. Equireflectionality in Acoustic Waveguide Networks

Let us now investigate the scattering properties of the system by connecting the points a and b to two waveguides with the same cross-section, as shown in Fig. 2(b). For this setup, the two incoming plane waves can be related to the outgoing waves through Eq. (1). To find the corresponding scattering coefficients we first relate the acoustic pressure and its derivative between points a and b through a matrix involving the eigenmodes of the closed cavity. To do so, we use the integral formalism with an expression of the Green function of the closed cavity. Then, as explained in detail in section IV of the supplemental material of [13], it can be shown that the former matrix is mirror symmetric due to the point-wise parity of the eigenmodes. This leads to equireflerectionality $r_1 = r_2$ of the corresponding scattering problem and thus the surprising result of Fig. 1 (d).

So far, we have focussed on the case of thin waveguides. When deviating from this limiting case of $w \ll L$, 3D-effects at the junctions of the waveguides will play a role due to evanescent waves; their severity is, clearly, system-dependent (number of junctions, geometry of the connection etc). We calculated the reflection coefficients for various values of w/L and show some characteristic results in Fig. 3. In particular we show the reflections $r_1(f), r_2(f)$ for the latently-symmetric scattering network of Fig. 1 (d). As can be seen, for this setup, $r_1 = r_2$ holds quite well even when w/L is far from the limiting value zero, although some deviations are seen in Fig. 3 (b). In Fig. 3(c) we show a more quantitative comparison of the behavior of these two reflections by showing the absolute value of the frequency-dependent difference $r_1(f) - r_2(f)$ for different sidelengths w. In all of the calculations for Fig. 3, we have used viscothermal losses, which, as can be seen, do not alter equireflectionality. Indeed, it turns out that this kind of losses does not at all impact the latent symmetry of the cavity or the equireflectionality of the (open) system (see Appendix C for details).

We stress that the network depicted in Fig. 1 (d) is, by far, not the only one with latent symmetry-induced equireflectionality. Indeed, as we show in the following, one can easily generate a plethora of such networks.

Perhaps the easiest approach is to generate a large number of different networks and test each of them for latent symmetry. Opening the network at two latently symmetric points will then lead to equireflectional scattering.

Crucially, both of these tasks—generating networks and testing for latent symmetry—can be efficiently done. For the first task, it is important to remember the following: Since we work with strictly one-dimensional (single-mode) waveguides, the actual geometry of the network is not of importance. Instead, what matters is only how the waveguides are interconnected; that is, the network's topology. Mathematically speaking, our waveguide networks are nothing but so-called simple graphs, which are extensively treated in graph theory [28]. This conceptual overlap allows us to lend tools from graph theory; in particular, we can rely on the powerful nauty suite [29]. With nauty, generating a large number of networks is rather efficient; for instance, generating all 11,716,571 distinct waveguide networks with $N = 10$ sites takes less than 10 seconds on a modern laptop [30]. For the second step, we need to check each of the obtained networks for latent symmetries. To this end, one needs to build the matrices A, B, H. Checking whether the network has a latent symmetry then boils down to computing the first $N-1$ matrix powers and checking whether there are sites a, b that fulfill Eq. (4). In this manner, a plethora of possible networks can be found. Some examples are shown in Fig. 4.

D. Experimental Observation in Microwave Transmission-Line Networks

As mentioned earlier, besides acoustic waveguide networks, microwave transmission-line networks lend themselves well to experimentally observe the discussed scattering signature of latent symmetry, namely equireflec-

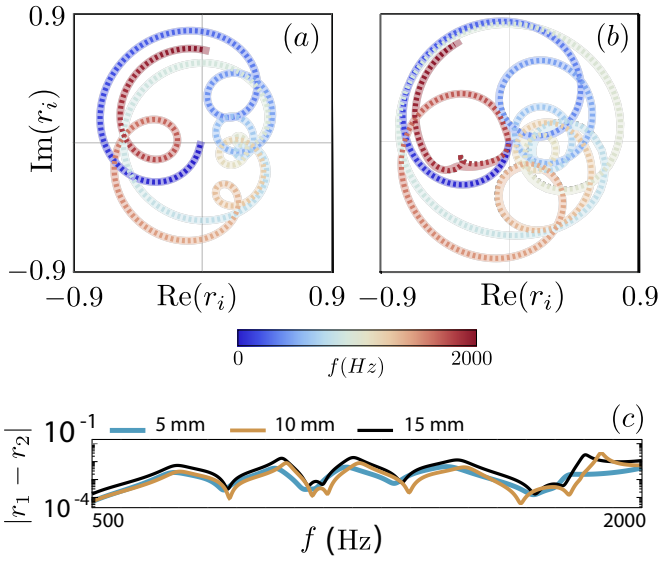

Figure 3. Results from $3D$ finite-element simulations of scattering off the structure of Fig. 1(d) using COMSOL, with visco-thermal losses modelled through the "narrow region acoustics" function. The waveguides are identical with a length of $L = 0.1m$, and with a quadratic cross-section with side length w. (a) and (b) show a comparison of r_1 (solid line) and r_2 (dashed line) for waveguide side lengths $w = 5mm$ and $w = 15mm$, respectively. The frequency range is between 0 and $2000Hz$, which comprises a little more than the first 12 eigenmodes of the underlying cavity. (c) Comparison of $|r_1 - r_2|$ for three values of w.

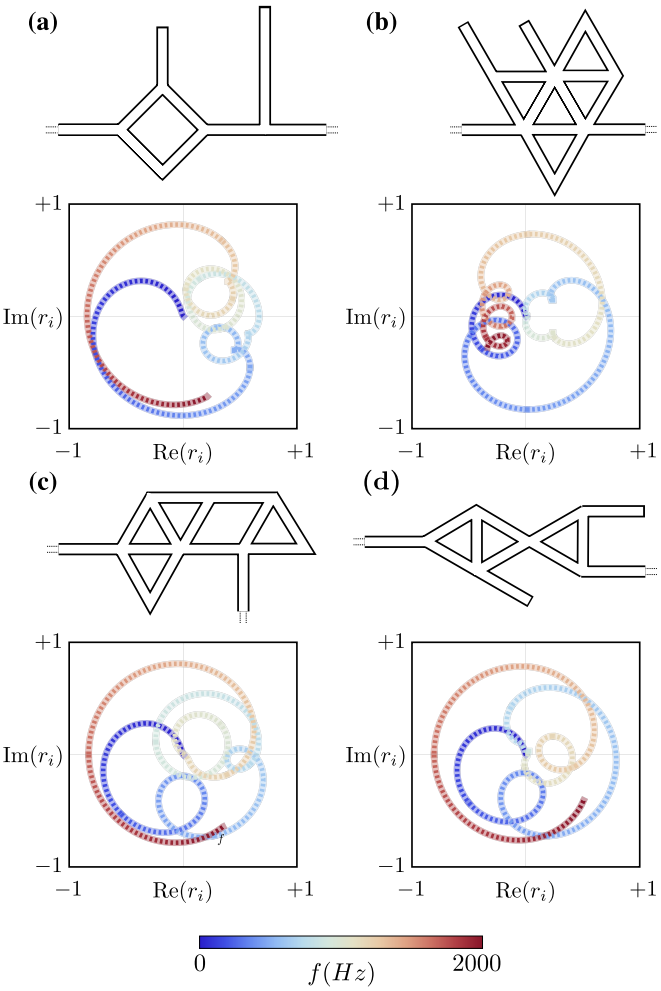

Figure 4. Different waveguide networks whose scattering matrix is equireflectional. Just as in Fig. 1, the reflection coefficents are computed for each network and plotted (in the complex plane) below each network. Since the networks are equireflectional, the two curves $r_1(f)$ (solid line) and $r_2(f)$ (dashed line) are identical. The reflection coefficents have been computed with the same parameters as in Fig. 1, though now up to $f = 2000\,Hz$.

tion. Indeed, as can be easily shown [23, 24, 31], the mathematical considerations in Section II B can be directly applied to transmission-line networks, if only we replace the pressure field p with the voltage U. The only difference between the two platforms is that, in acoustics, a waveguide with a closed end (acoustic hard wall) features Neumann boundary conditions on that end; to achieve the same in transmission line networks, we need to make the corresponding cable *open-ended*. In summary, and taking into account this correspondence, the structures with latent symmetry from Fig. 1(d) and Fig. 4 are directly applicable to a microwave realization.

We have hence built the networks from Fig. 1(d) and Fig. 4(a) using 50 cm-long coaxial cables and measured their scattering parameters with a vector network analyzer (VNA, Rhode & Schwarz ZVA 67, 10 MHz – 67 GHz). The finite propagation delay in the junctions is equivalent to the case of point-like junctions with slightly longer waveguides. The latter is in line with our theoretical model. We also make sure that the effective length of each waveguide is identical.

We observe in Fig. 5 excellent agreement of the complex-valued reflection coefficients (i.e., in terms of both magnitude and phase) with the expected equireflection condition at all frequencies. Moreover, a clear periodicity of the reflection spectrum is visible. Furthermore, it is apparent that the absorption strength increases monotonously with frequency, as expected.

III. POWERS OF THE SCATTERING MATRIX AND PERFECT ABSORPTION

Although two-port systems provide an intuitive and simple setup to study wave scattering, many applications are actually based on N-port configurations (circulators, splitters, multiplexers etc.). In view of these implementations, in this Section, we study latent symmetry and generalisations of it *directly on the scattering matrix itself* and not on the underlying structure. In such a way the results obtained here do not depend on the specific physical system and are rather general for any N-port scattering matrix S.

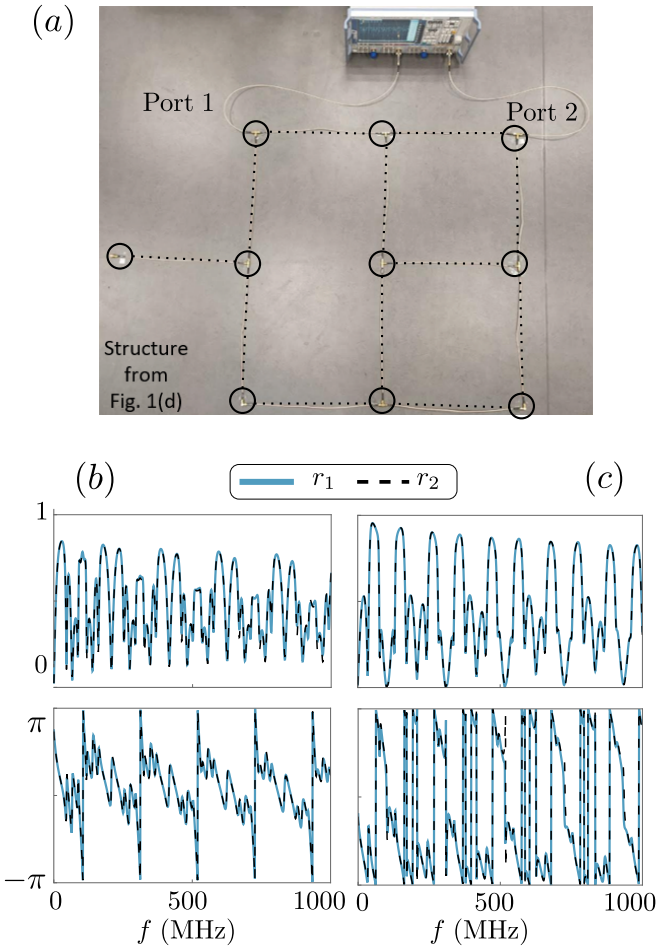

Figure 5. Experimental scattering measurements on microwave transmission-line networks with latent symmetry. (a) Photography of the experimental setup for the network from Fig. 1(d). (b) and (c) Magnitude and phase of the measured reflection coefficients for the networks from Fig. 1(d) and Fig. 4(a), respectively.

We first note that any reciprocal scattering matrix is symmetric $S = S^T$. Let us then consider a case where this matrix is also latently symmetry; that is, it fulfills

$$(S^m)_{a,a} = (S^m)_{b,b}\,, \quad \forall \quad m = 1, \ldots, N \tag{5}$$

for some a and b. Note that this relation for $m = 1$ implies that ports a and b have the same reflection coefficient. We emphasize that the connection between matrix powers, cospectrality and eigenvectors (presented in the last section) is valid for the scattering matrix as well. Thus, if Eq. (5) is valid, the eigenvectors of the S matrix will have parity between the elements a and b. However, the eigenvectors of the scattering matrix, except for particular cases (as we show below) are not so useful. We remind the reader that Eq. (5) also implies cospectrality between $S \setminus a$ and $S \setminus b$ but gives no information about the eigenvalues of S itself. To bypass this, let us go one step further and generalise Eq. (5) by introducing the following relation

$$(S^m)_{a,a} = c \cdot (S^m)_{b,b} \quad \forall \quad m = 1, \ldots, N\,. \tag{6}$$

We call this relation, Eq. (6), *scaled cospectrality* of a matrix S with a scaling factor c. Interestingly, this rather simple generalisation has direct impact on the eigenvalues of the matrix S: whenever $c \neq 1$, scaled cospectrality enforces the existence of one zero eigenvalue (more zeros might appear accidentally). To show why this is the case, let us start by realizing that, from the Cayley-Hamilton theorem, we know that S^N can be written as a polynomial in the first $N-1$ powers of S, that is,

$$S^N = -\sum_{m=0}^{N-1} a_m S^m\,, \tag{7}$$

where $S^0 \equiv I$ is the identity matrix and where the coefficients a_m are taken from the characteristic polynomial of S, given by $P(x) = \det(x\,I - S) = \sum_{m=0}^{N} a_m x^m$. Now, since the matrix S fulfills $\left(S^N\right)_{a,a} = c\left(S^N\right)_{b,b}$, it follows from Eq. (7) that

$$-a_0 I_{a,a} - \sum_{m=1}^{N-1} a_m \left(S^m\right)_{a,a} = c\left(-a_0 I_{b,b} - \sum_{m=1}^{N-1} a_m \left(S^m\right)_{b,b}\right) \tag{8}$$

from which we get

$$a_0\,(I)_{a,a} = c\,a_0\,(I)_{b,b}\,. \tag{9}$$

It follows that $a_0 = 0$ whenever $c \neq 1$ and since a_0 is proportional to the determinant of S, we see that S has to have a vanishing eigenvalue. The existence of a zero eigenvalue of S directly implies that there must be a monochromatic adapted wavefront that can be injected at the real frequency at which S has the zero eigenvalue such that it is perfectly absorbed within the system [32]. This CPA requires the system to have a finite amount of absorption loss and hence a sub-unitary S matrix. Indeed, in the absence of any absorption loss, the S matrix would be unitary and the magnitude of its determinant would be unity, implying that a_0 cannot be zero because a_0 is proportional to $\det(S)$.

Let us remark for the interested reader that in the literature there is also another generalization of cospectrality, the so-called *fractional cospectrality* [33], which, however, does not enforce the presence of a zero eigenvalue.

In this section, we have so far not explicitly stated the frequency dependence of S. However, a scattering system can in general only fulfill the conditions for scaled cospectrality at discrete frequencies, which is hence in line with the fact that the zeros of S only occur at discrete (potentially complex) frequencies. In other words, if one optimizes the scattering system such that it has scaled cospectrality (and thus CPA) at some frequency f_0, there is no reason to expect scaled cospectrality at any frequency other than f_0.

In the remainder of this section, we will show that systems with scaled cospectrality allow us to achieve CPA with wavefronts that have a customized imbalance in terms of the weights of different channels. Before explaining the origin of this feature in detail, let us briefly contextualize this feature within the recent literature on achieving CPA. The S matrix of a generic (arbitrarily complex) scattering system does not necessarily have a zero eigenvalue, but can be tuned to have one [19, 32, 34, 35]. With sufficient tunable degrees of freedom, the real frequency at which the zero eigenvalue occurs can be controlled, too [17, 36, 37]. However, in structures without symmetry the required CPA wavefront is in general highly asymmetrical and difficult to generate [38]. This makes it more challenging to realize the envisaged use of CPA to interferometrically control light with light, and hence without any non-linearity [39, 40]. A generic way to impose CPA at a desired frequency and with an arbitary CPA wavefront was demonstrated in Ref. [20] by tuning a massively parametrized chaotic cavity. Here, we provide an alternative route through scaled cospectrality to obtain structures featuring CPA whose wavefront has a prescribed imbalance. Thereby, only a weak control wave can modulate a strong signal, provided that the necessary phase and amplitude relation between the two is respected.

We now illustrate the above results with an implementation of the scaled cospectrality using a particular example of a 3-port acoustic network with lossy acoustic waveguides (see Appendix C for details). For simplicity we choose to work with an extension of the 2-port system of the previous section by symmetrically coupling an arbitrary structure to a and b as shown in Fig. 6 (a). The symmetric connection and the added structure are highlighted by light gray and dark gray respectively.

The two latently symmetric points are symmetrically connected to ports 1 and 2, and thus the scattering matrix of the 3-port network reads

$$S = \begin{pmatrix} r & t & t' \\ t & r & t' \\ t' & t' & r' \end{pmatrix}. \tag{10}$$

with r, r' denoting reflection coefficients, and with t, t' transmission coefficients. Evidently the proposed design ensures the equireflectionality (r) of the two symmetric ports 1 and 2 while an additional reflection (r') from port 3 is introduced. Due to reciprocity and symmetry we are thus left with only two different transmission coefficients t and t'. For this particular matrix we impose scaled cospectrality between ports 1 (or equivalently 2) and 3 by demanding that it satisfies Eq. (6). Note that for $m = 1$ we simply get a scaling between the reflections, $r = cr'$. Then, solving for the higher powers we obtain two possible solutions which are discussed in the following.

CPA without any zero-input channel: One solution requires

$$t = -r'/2, \text{ and } t' = r'\sqrt{2c-1}/2\,. \tag{11}$$

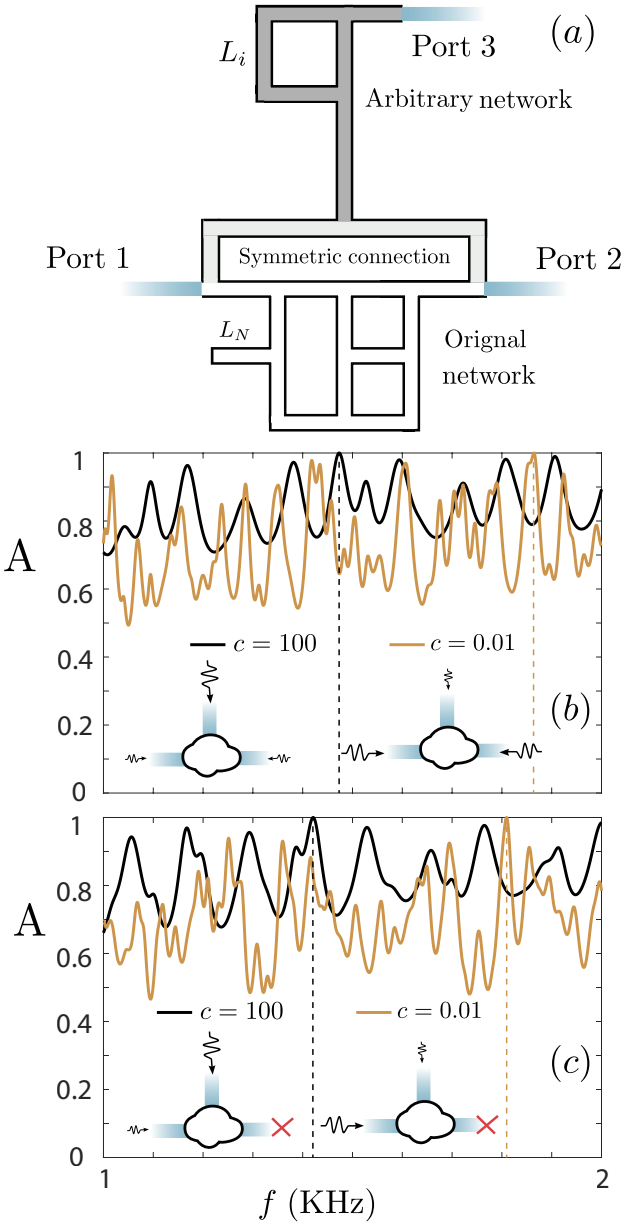

Figure 6. (a) A symmetric extension of the 2-port setup shown in Fig. 1 (d). For (b) and (c), we finetune the lengths of the acoustic waveguides of the network (a) to fulfill scaled cospectrality between ports 1 and 3 with the scattering matrix fulfilling either Eq. (11) [for (b)] or Eq. (15) [for (c)]. For each (b) and (c), we show the frequency-dependent absorption A of the network for the two different choices $c = 100$ and $c = 1/100$.

To illustrate the effects of the zero eigenvalue of S and its relation to CPA, we define the following eigenvalue problem

$$S\mathbf{x} = \lambda\mathbf{x}. \tag{12}$$

When S satisfies Eq. (11), the corresponding eigenvalues of the scattering matrix are $\lambda_1 = (0, (c+1/2)r', (c+1/2)r')$. As expected by our definition of the generalised

cospectrality, the scattering matrix acquires a zero eigenvalue. This zero eigenvalue implies that if one uses as an input the corresponding eigenvector, the output is *zero* and the input wavefront is perfectly absorbed. In fact, here the corresponding eigenvector is

$$\mathbf{x}_1 = (-1/\sqrt{2c-1}, -1/\sqrt{2c-1}, 1)^T . \tag{13}$$

Importantly, the imbalance of the input wavefront is solely controlled by the scaling factor c which we can prescribe.

In order to validate our results, we once again consider the case of airborne acoustic waveguides including viscothermal losses. The elements of the S matrix in such a case can be calculated using different techniques such as the star product (see Appendix E for details). We optimize the lengths of several parts of the network (while maintaining the symmetry between ports 1 and 2) such that Eq. (11) is satisfied for a predefined value of c and a suitable frequency $\overline{f}_1$. To illustrate our result, we assume an input to the 3-port network in the form of a vector $\mathbf{p}_{\text{in}} = \mathbf{x}_1$ and thus the output vector is naturally given by $\mathbf{p}_{\text{out}} = S\,\mathbf{p}_{\text{in}}$. Using the output we can calculate absorption from such networks as

$$A \equiv 1 - \frac{|\mathbf{p}_{\text{out}}|^2}{|\mathbf{p}_{\text{in}}|^2}. \tag{14}$$

The absorption for two different networks is shown in Fig. 6(b). The black thick (orange thin) line corresponds to a network satisfying Eq. (11) with $c = 100$ ($c = 0.01$). The details of the geometry of the obtained networks are given in Appendix E. According to our design, at the prescribed frequency $\overline{f}_1$, CPA of the input wave is achieved, indicated by $A = 1$. We additionally observe that with relatively small variations of the lengths of the waveguides (see Appendix E), we achieve CPA for a very different input vector of an amplitude 10 times larger (smaller) for port 1/2 compared to port 3.

CPA with one zero-input channel: The other possible solution for S to acquire scaled cospectrality is when

$$t = r = cr' \text{ and } t' = \sqrt{c}r' , \tag{15}$$

with the eigenvalues of S then being $\lambda_2 = (0, 0, (2c+1)r')$. The corresponding eigenvectors of the two zero eigenvalues are $\mathbf{x}_2^{(1)} = (1, -1, 0)^T$ and $\mathbf{x}_2^{(2)} = (1, 1, -2\sqrt{c})^T$. This case is even more interesting since it features a two-fold degenerate zero eigenvalue [41]. Consequently, for any choice of α, β, inputs of the form $\alpha\mathbf{x}_2^{(1)} + \beta\mathbf{x}_2^{(2)}$ will be perfectly absorbed. Among all possible inputs, one can find the following highly asymmetric one:

$$\mathbf{x}_2 = (-1, 0, \sqrt{c})^T . \tag{16}$$

Thus, the 3-port network is able to completely absorb waves with non-zero inputs on only two of its ports and with a relative input between the two active ports prescribed by the scale factor c. We have constructed two such networks using $c = 100$ and $c = 0.01$, satisfying Eq. (15) at a prescribed frequency $\overline{f}_2$ and the corresponding absorption is shown in Fig. 6(c) using the input $\mathbf{p}_{in} = \mathbf{x}_2$. The networks feature CPA ($A = 1$) at the desired frequency $\overline{f}_2$ with non-zero inputs in only two of the three channels. On top of that, the imbalance of the CPA wavefront introduced by the scale factor c results in an almost single sided (or one port) CPA.

IV. CONCLUSIONS

We have studied the scattering properties of various asymmetric waveguide networks and demonstrated that a certain family of networks possesses the same scattering properties as mirror-symmetric ones, i.e. they show equireflectionality. This counterintuitive property of the asymmetric networks stems from a hidden mirror symmetry called latent symmetry. We have validated this finding numerically for acoustic waveguide networks and experimentally for microwave transmission-line networks.

While latent symmetry is mathematically equivalent to certain relations obeyed by the matrix powers, here we generalized these relations and applied them to a generic scattering matrix of an N-port system. The new relations, named scaled cospectrality, were then used to construct networks featuring CPA. Specifically, a scaling factor was used to design systems able to completely absorb wavefronts with prescribed imbalance, a capability that can enable the control of light with a very weak coherent control signal. Overall, our work demonstrates that scattering problems may greatly profit from the notion of latent symmetry—which has very recently been experimentally tested also in non-reciprocal networks [42]—and of matrix power relations in general.

ACKNOWLEDGMENTS

The authors are thankful to M. Pyzh and V. Pagneux for valuable discussions. V.A. acknowledges financial support from the NoHeNA project funded under the program Etoiles Montantes of the Region Pays de la Loire. V. A. is supported by the EU H2020 ERC StG “NASA” Grant Agreement No. 101077954.

[1] M. E. Peskin, *An Introduction to Quantum Field Theory*, 1st ed. (CRC Press, Boca Raton, 2018).

[2] B. D. Cullity and S. R. Stock, *Elements of X-Ray Diffraction*, 3rd ed. (Pearson, 2001).

[3] *Introduction to Wave Scattering, Localization and Mesoscopic Phenomena*, 2nd ed. (Springer-Verlag Berlin Heidelberg, 2006).

[4] H. A. Macleod, *Thin-Film Optical Filters*, 4th ed., Series in Optics and Optoelectronics (CRC Press/Taylor & Francis, Boca Raton, FL, 2010).

[5] E. Dokumacı, *Duct Acoustics: Fundamentals and Applications to Mufflers and Silencers* (Cambridge University Press, Cambridge, 2021).

[6] Thomas D. Rossing, ed., *Springer Handbook of Acoustics*, 2nd ed., Springer Handbooks (Springer New York, NY, 2015).

[7] D. Smith and B. Webb, Hidden symmetries in real and theoretical networks, Physica A **514**, 855 (2019).

[8] M. Kempton, J. Sinkovic, D. Smith, and B. Webb, Characterizing cospectral vertices via isospectral reduction, Linear Algebra Its Appl. **594**, 226 (2020).

[9] M. Röntgen, *Latent Symmetries: An Introduction*, Other (MetaMAT Weekly Seminars, 2022).

[10] L. Bunimovich and B. Webb, *Isospectral Transformations: A New Approach to Analyzing Multidimensional Systems and Networks*, 1st ed., Springer Monographs in Mathematics (Springer, New York, NY, United States, 2014).

[11] M. Röntgen, M. Pyzh, C. V. Morfonios, N. E. Palaiodimopoulos, F. K. Diakonos, and P. Schmelcher, Latent symmetry induced degeneracies, Phys. Rev. Lett. **126**, 180601 (2021).

[12] C. V. Morfonios, M. Pyzh, M. Röntgen, and P. Schmelcher, Cospectrality preserving graph modifications and eigenvector properties via walk equivalence of vertices, Linear Algebra Its Appl. **624**, 53 (2021).

[13] M. Röntgen, C. V. Morfonios, P. Schmelcher, and V. Pagneux, Hidden Symmetries in Acoustic Wave Systems, Phys. Rev. Lett. **130**, 077201 (2023).

[14] M. Röntgen, M. Pyzh, C. V. Morfonios, and P. Schmelcher, On symmetries of a matrix and its isospectral reduction, arXiv:2105.12579 (2021).

[15] Y. D. Chong, L. Ge, H. Cao, and A. D. Stone, Coherent perfect absorbers: Time-reversed lasers, Phys. Rev. Lett. **105**, 053901 (2010).

[16] N. I. Landy, S. Sajuyigbe, J. J. Mock, D. R. Smith, and W. J. Padilla, Perfect metamaterial absorber, Phys. Rev. Lett. **100**, 207402 (2008).

[17] M. F. Imani, D. R. Smith, and P. del Hougne, Perfect absorption in a disordered medium with programmable meta-atom inclusions, Adv. Funct. Mater. **30**, 2005310 (2020).

[18] W. Wan, Y. Chong, L. Ge, H. Noh, A. D. Stone, and H. Cao, Time-reversed lasing and interferometric control of absorption, Science **331**, 889 (2011).

[19] K. Pichler, M. Kühmayer, J. Böhm, A. Brandstötter, P. Ambichl, U. Kuhl, and S. Rotter, Random anti-lasing through coherent perfect absorption in a disordered medium, Nature **567**, 351 (2019).

[20] P. del Hougne, K. B. Yeo, P. Besnier, and M. Davy, Coherent wave control in complex media with arbitrary wavefronts, Phys. Rev. Lett. **126**, 193903 (2021).

[21] T. Kottos and U. Smilansky, Quantum graphs: A simple model for chaotic scattering, J. Phys. A: Math. Gen. **36**, 3501 (2003).

[22] G. Berkolaiko and P. Kuchment, *Introduction to Quantum Graphs*, Mathematical Surveys and Monographs, Vol. 186 (American Mathematical Society, 2013).

[23] O. Hul, S. Bauch, P. Pakoński, N. Savytskyy, K. Życzkowski, and L. Sirko, Experimental simulation of quantum graphs by microwave networks, Phys. Rev. E **69**, 056205 (2004).

[24] T. Hofmann, J. Lu, U. Kuhl, and H.-J. Stöckmann, Spectral duality in graphs and microwave networks, Phys. Rev. E **104**, 045211 (2021).

[25] A. Coutant, V. Achilleos, O. Richoux, G. Theocharis, and V. Pagneux, Topological two-dimensional Su–Schrieffer–Heeger analog acoustic networks: Total reflection at corners and corner induced modes, J. Appl. Phys. **129**, 125108 (2021).

[26] A. Coutant, A. Sivadon, L. Zheng, V. Achilleos, O. Richoux, G. Theocharis, and V. Pagneux, Acoustic Su-Schrieffer-Heeger lattice: Direct mapping of acoustic waveguides to the Su-Schrieffer-Heeger model, Phys. Rev. B **103**, 224309 (2021).

[27] O. Richoux, V. Achilleos, G. Theocharis, I. Brouzos, and F. Diakonos, Multi-functional resonant acoustic wave router, J. Phys. D: Appl. Phys. **53**, 235101 (2020).

[28] M. Newman, *Networks: An Introduction*, 2nd ed. (Oxford University Press, Oxford, 2018).

[29] B. D. McKay and A. Piperno, Practical graph isomorphism, II, J. Symb. Comput. **60**, 94 (2014).

[30] To be precise, this number includes only the graphs which are connected. In the context of waveguide networks, this means that the network does not contain parts which are disconnected from each other.

[31] Ahmed Mubarack, *Transmission Lines, Quantum Graphs and Fluctuations on Complex Networks*, Ph.D. thesis, University of Nottingham (2021).

[32] L. Chen, T. Kottos, and S. M. Anlage, Perfect absorption in complex scattering systems with or without hidden symmetries, Nat. Commun. **11**, 5826 (2020).

[33] A. Chan, G. Coutinho, W. Drazen, O. Eisenberg, C. Godsil, M. Kempton, G. Lippner, C. Tamon, and H. Zhan, Fundamentals of fractional revival in graphs, Linear Algebra and its Applications **655**, 129 (2022).

[34] Y. V. Fyodorov, S. Suwunnarat, and T. Kottos, Distribution of zeros of the S-matrix of chaotic cavities with localized losses and coherent perfect absorption: Non-perturbative results, J. Phys. A: Math. Theor. **50**, 30LT01 (2017).

[35] H. Li, S. Suwunnarat, R. Fleischmann, H. Schanz, and T. Kottos, Random matrix theory approach to chaotic coherent perfect absorbers, Phys. Rev. Lett. **118**, 044101 (2017).

[36] B. W. Frazier, T. M. Antonsen, S. M. Anlage, and E. Ott, Wavefront shaping with a tunable metasurface: Creating cold spots and coherent perfect absorption at arbitrary frequencies, Phys. Rev. Res. **2**, 043422 (2020).

[37] P. del Hougne, K. B. Yeo, P. Besnier, and M. Davy, On-Demand Coherent Perfect Absorption in Complex Scattering Systems: Time Delay Divergence and Enhanced

Sensitivity to Perturbations, Laser & Photonics Reviews **15**, 2000471 (2021).
[38] See Supplementary Note 4 in Ref. [43] for a detailed analysis in terms of entropy and participation number of CPA wavefronts in a chaotic cavity.
[39] J. Zhang, K. F. MacDonald, and N. I. Zheludev, Controlling light-with-light without nonlinearity, Light Sci. Appl. **1**, e18 (2012).
[40] D. G. Baranov, A. Krasnok, T. Shegai, A. Alù, and Y. Chong, Coherent perfect absorbers: linear control of light with light, Nat. Rev. Mater. **2**, 1 (2017).
[41] J. R. Piper, V. Liu, and S. Fan, Total absorption by degenerate critical coupling, Appl. Phys. Lett. **104**, 251110 (2014).
[42] J. Sol, M. Röntgen, and P. del Hougne, Covert Scattering Control in Metamaterials with Non-Locally Encoded Hidden Symmetry (2023), arxiv:2305.00906 [physics].
[43] J. Sol, A. Alhulaymi, A. D. Stone, and P. del Hougne, Reflectionless programmable signal routers, Science Advances **9**, eadf0323 (2023).
[44] CW. Kosten and C. Zwikker, *Sound Absorbing Materials* (Elsevier Amsterdam, 1949).

Appendix A: Formula for the scattering matrix

In the following, we describe how the scattering matrix of the waveguide networks (assuming one-dimensional waveguides) can be computed. The expressions are taken from [21]. Technically, they rely on describing the network in terms of a so-called quantum graph with Neumann vertex conditions.

Given the topology matrix A describing the waveguide network (see main text), and the diagonal matrix B with entries $B_{i,i} = \sum_j A_{i,j}$, we define the two matrices

$$h(k) = \frac{A}{\sin(kL)} - \frac{B}{\tan(kL)} \tag{A1}$$

and the $2 \times N$ coupling matrix W whose elements are all zero, except $W_{1,a} = W_{2,b} = 1$. L denotes the length of the individual waveguides, and k is the (complex) wavenumber.

The scattering matrix can be shown to be given by [21]

$$S(k) = 2iW \left(h(k) + iW^T W\right)^{-1} W^T - \mathbf{I} \tag{A2}$$

where $\mathbf{I}$ is the 2×2 identity matrix.

Appendix B: Eigenvectors of symmetric scaled cospectral matrices

Let $S = S^T \in \mathbb{C}^{N\times N}$ be a complex-symmetric matrix, and let us assume that $(S^m)_{a,a} = c \cdot (S^m)_{b,b}$ for all $m > 0$. It follows that

$$\left(e^{iSt} - 1\right)_{a,a} = c \cdot \left(e^{iSt} - 1\right)_{b,b}. \tag{B1}$$

We assume that S has no degenerate eigenvalues, which in particular implies that S is diagonalizable. Then, since $S = S^T$, one can normalize its eigenvectors $|\phi_i\rangle$ such that $\langle\phi_j^*|\phi_i\rangle = \delta_{i,j}$ with the star denoting the complex conjugate. As a consequence, we have $1 = \sum_i |\phi_i\rangle \langle\phi_i^*|$. Equipped with this identity, we get

$$\left(e^{iSt} - 1\right)_{a,a} = \sum_{i,j} \langle a|\phi_i\rangle \langle\phi_i^*|e^{iSt}|\phi_j\rangle \langle\phi_j^*|a\rangle - 1 \tag{B2}$$

$$= \sum_i \langle a|\phi_i\rangle e^{i\lambda_i t} \langle\phi_i^*|a\rangle - 1 \tag{B3}$$

$$= c \cdot \left(\sum_i \langle b|\phi_i\rangle e^{i\lambda_i t} \langle\phi_i^*|b\rangle - 1\right) \tag{B4}$$

with λ_i being the eigenvalue of $|\phi_i\rangle$. Since the complex exponentials are linearly independent, one can evaluate the above equation independently for each distinct λ_i, so that it automatically follows that

$$\langle a|\phi_i\rangle \langle\phi_i^*|a\rangle = c \cdot \langle b|\phi_i\rangle \langle\phi_i^*|b\rangle, \quad \lambda_i \neq 0 \tag{B5}$$

$$\langle a|\phi_0\rangle \langle\phi_0^*|a\rangle = c \cdot \langle b|\phi_0\rangle \langle\phi_0^*|b\rangle - c + 1, \quad \lambda_0 = 0. \tag{B6}$$

Since $\langle\phi_j^*|a\rangle = \langle a|\phi_j\rangle$ for *all* eigenvectors, we obtain

$$\langle a|\phi_i\rangle = \pm\sqrt{c} \cdot \langle b|\phi_i\rangle, \quad \lambda_i \neq 0 \tag{B7}$$

$$\left(\langle a|\phi_0\rangle\right)^2 = c \cdot \left(\langle b|\phi_0\rangle\right)^2 - c + 1, \quad \lambda_0 = 0. \tag{B8}$$

Appendix C: Equireflectionality in a lossy system

In the main text of this work, we considered the case of latent reflection symmetry in a system without losses, and we mentioned that the point-wise parity of eigenmodes remains valid for the case of losses in the one-dimensional waveguides described by a complex velocity $c = c_r + ic_i$. In the following, we give the justification for this statement.

To this end, let us assume that we have a network which, in the absence of losses, has a latent reflection symmetry between two junctions a, b. As stated in the main text, for low-enough frequencies, the eigenmodes of this network can be found from the generalized eigenvalue problem

$$A\,\boldsymbol{\phi} = \cos(kL) B\,\boldsymbol{\phi} \tag{C1}$$

where $\boldsymbol{\phi}$ contains the pressure of the eigenmode ϕ at the N junctions of the network, and with $k = \omega/c = \omega/c_r \equiv k_r$. The eigenvalues $\cos(kL)$ of this problem are completely real and due to latent symmetry, all eigenmodes fulfill $p_a = \pm p_b$.

Let us then take the usual route for introducing losses: That is, we start from the lossless case—as described through Eq. (C1)—and then let the velocity $c = c_r + ic_i$ (due to, in particular, thermo-viscous boundary at the surface of the one-dimensional waveguides [44]). Obviously, this changes the relation between k and ω, but it does not change the eigenvalues $\cos(kL)$ or the eigenvectors $\boldsymbol{\phi}$. In other words, each eigenvector $\boldsymbol{\phi}$ with eigenvalue $\cos(kL)$ of the lossless system will still be an eigenvector of the lossy system, with unchanged eigenvalue $\cos(kL)$. In particular, point-wise parity of eigenmodes is preserved. What changes is the frequency ω corresponding to $\cos(kL)$: Since c is complex while k is real (as imposed from the fact that $\cos(kL)$ is real), ω is in general complex as well, with the imaginary part being related to the lifetime of this lossy eigenmode.

Appendix D: Using the matrix power relations for deriving a better understanding of latently symmetric waveguide networks

The aim of this section is to showcase a set of intuitive and easily interpretable equivalent conditions that the relations Eq. (4)—latent symmetry, that is—impose on a waveguide network. These conditions can be derived by analyzing Eq. (4) order by order and subsequently using the relation $H = B^{-1/2}AB^{-1/2}$ to derive conditions on the matrices A, B which are directly describing the underlying waveguide network. We restrict ourselves to the first few orders of Eq. (4), for which the corresponding equivalent conditions have been derived in [13]; we repeat them here for self-containedness of the present manuscript.

The conditions are then as follows. Firstly, a and b have to have the same number of neighbors. Moreover, in the special case where the number of next-neighbors of a, b is equal to unity, (i) Eq. (4) holds for $m = 2$ if and only if a, b have the same number of next-neighbors, and (ii) Eq. (4) holds for $m = 3$ if and only if

$$\sum_{i\in\mathcal{N}^2(a)} \frac{1}{|\mathcal{N}(i)|} = \sum_{i\in\mathcal{N}^2(b)} \frac{1}{|\mathcal{N}(i)|}\,. \tag{D1}$$

In this relation, $\mathcal{N}^2(i)$ denotes the set of next-neighbors of i, and $|\mathcal{N}(i)|$ denotes the degree of site i, that is, the number of neighbors of i.

Equipped with the above, we can now analyse the difference between the setups shown in Fig. 1 (c) and Fig. 1 (d) in more detail. To this end, let us close these two systems on the entry-points of the two ports, and call these points a (on the left-hand side of the setup) and b (on the right-hand ride of the setup); compare Fig. 2.

For the asymmetric network of Fig. 1 (c), the two next-neighbors of a have degrees 3 and 2, while the two next-neighbors of b both have degree 3. Thus, the equation Eq. (D1) is not fulfilled and, as a consequence, the relations Eq. (4) are not fulfilled for $m = 3$. On the other hand, the setup of Fig. 1 (d) features an additional waveguide on the left, which equalized the two sides of Eq. (D1).

Appendix E: Optimization procedure and lengths of the optimized structures

In order to design a system whose scattering matrix has the form of Eq. (10) and which fulfills either Eq. (15) or Eq. (11), we proceed as follows: We started with the system depicted in Fig. 6 (a), whose scattering matrix has the structure of Eq. (10). We then optimized the lengths $L_1, \ldots, L_5$ (see Fig. 7) and the frequency f in the range between 1000 and 2000 Hz such that Eqs. (11) and (15) are fulfilled, respectively, at a frequency $\overline{f}$. Technically, we modeled the system as a network of ideal waveguides of length L_m, each with a transmission coefficient

$$t_m = exp(-ikL_m) \tag{E1}$$

with

$$k = \frac{2\pi f}{c_s} + (1+i)\,\alpha\,\frac{\sqrt{f}}{R}; \tag{E2}$$

where α is the loss coefficient (see below) [44], $R = 1\,cm$ the waveguide diameter, with $c_s = 343\,m/s$ the velocity of sound and f being the frequency. Using the continuity of the pressure and the conservation of the flux at each junction, we then obtain the scattering matrix S, depending only on the frequency f and the lengths L_m.

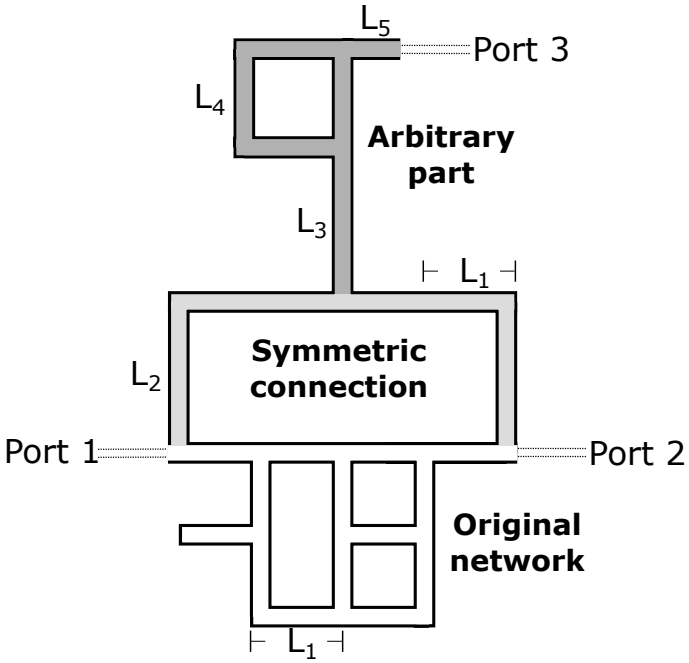

Figure 7. Reference figure showing the assignment of the waveguide lengths $L_1, \ldots, L_5$.

The optimized lengths (in meters, rounded to 4 digits after the decimal point) are shown in the table below. The cases a and b correspond to the scattering matrix fulfilling Eq. (11) and Eq. (15) of the main text, respectively.

	case a, $c = 1/100$	case a, $c = 100$	case b, $c = 1/100$	case b, $c = 100$
L_1	0.7976	0.1021	0.7792	0.1326
L_2	0.6398	0.6003	0.3944	0.7917
L_3	0.1070	0.3201	0.4018	0.6452
L_4	0.7497	0.8000	0.3357	0.7232
L_5	0.7837	0.7045	0.3289	0.5720

Appendix F: Confirming the reciprocity of the transmission line networks

In the main text, we have already shown the reflection coefficients for the transmission line measurements of the networks shown in Fig. 1(d) and Fig. 4(a). In Fig. 8, we also show the transmission coefficients, that is, the matrix elements $S_{1,2}$ and $S_{2,1}$ of the scattering matrix S. As can be seen, the networks are reciprocal in their scattering properties, that is, they fulfill $S_{1,2} = S_{2,1}$.

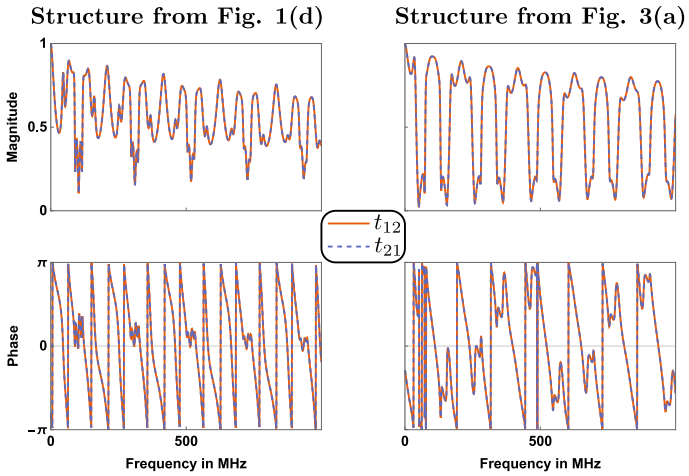

Figure 8. Experimentally measured transmission coefficients t_{ij} from port i to port j for the microwave transmission-line networks from Fig. 1(d) (left) and Fig. 4(a) (right).